



Measurements of low amounts of precipitable water vapor by millimeter wave spectroscopy: An intercomparison with radiosonde, Raman lidar, and Fourier transform infrared data

Irene Fiorucci,^{1,2} Giovanni Muscari,¹ Cesidio Bianchi,¹ Paolo Di Girolamo,³ Francesco Esposito,³ Giuseppe Grieco,³ Donato Summa,³ Giovanni Bianchini,⁴ Luca Palchetti,⁴ Marco Cacciani,⁵ Tatiana Di Iorio,⁵ Giulia Pavese,⁶ Domenico Cimini,⁷ and Robert L. de Zafra⁸

Received 15 January 2008; revised 19 May 2008; accepted 29 May 2008; published 31 July 2008.

[1] Observations of very low amounts of precipitable water vapor (PWV) by means of the Ground-Based Millimeter wave Spectrometer (GBMS) are discussed. Low amounts of column water vapor (between 0.5 and 4 mm) are typical of high mountain sites and polar regions, especially during winter, and are difficult to measure accurately because of the lack of sensitivity of conventional instruments to such low PWV contents. The technique used involves the measurement of atmospheric opacity in the range between 230 and 280 GHz with a spectral resolution of 4 GHz, followed by the conversion to precipitable water vapor using a linear relationship. We present the intercomparison of this data set with simultaneous PWV observations obtained with Vaisala RS92k radiosondes, a Raman lidar, and an IR Fourier transform spectrometer. These sets of measurements were carried out during the primary field campaign of the Earth Cooling by Water vapor Radiation (ECOWAR) project which took place at Breuil-Cervinia (45.9°N, 7.6°E, elevation 1990 m) and Plateau Rosa (45.9°N, 7.7°E, elevation 3490 m), Italy, from 3 to 16 March 2007. GBMS PWV measurements show a good agreement with the other three data sets exhibiting a mean difference between observations of $\approx 9\%$. The considerable number of data points available for the GBMS versus lidar PWV correlation allows an additional analysis which indicates negligible systematic differences between the two data sets.

Citation: Fiorucci, I., et al. (2008), Measurements of low amounts of precipitable water vapor by millimeter wave spectroscopy: An intercomparison with radiosonde, Raman lidar, and Fourier transform infrared data, *J. Geophys. Res.*, 113, D14314, doi:10.1029/2008JD009831.

1. Introduction

[2] Water vapor is a critical component of the atmosphere, plays a key role in the Earth's radiative balance and it is the most important atmospheric greenhouse gas because of its intense absorption of both shortwave and longwave radiation [e.g., Raval and Ramanathan, 1989; Held and Soden, 2000;

Marsden and Valero, 2004]. Accurate measurements of the atmospheric water distribution are therefore essential to adequately model Earth's radiation budget, with the column amount of water vapor (precipitable water vapor, or PWV) being one of the most important input parameters for atmospheric models [e.g., Clough et al., 1992].

[3] Of particular interest are regions characterized by very low atmospheric water vapor contents, such as polar regions. These regions are extremely vulnerable to present and projected climate changes and at the same time are the regions with the greatest potential to affect global climate [Solomon et al., 2007]. Obtaining accurate measurements of low amounts of PWV is especially important, for example, for modeling longwave radiative fluxes during polar winter months. Substantial variations in longwave emission caused by fluctuations in low amounts of water vapor directly affect the climate of polar regions through both greenhouse trapping of radiation and cloud formation processes. Yet, measurements of the low amounts of PWV observed during polar winters are difficult to achieve because of the required high instrumental sensitivity to water vapor [Cimini et al., 2007].

¹Istituto Nazionale di Geofisica e Vulcanologia, Rome, Italy.

²Also at Dipartimento di Fisica, Università di Bologna, Bologna, Italy.

³Dipartimento di Ingegneria e Fisica dell'Ambiente, Università della Basilicata, Potenza, Italy.

⁴Istituto di Fisica Applicata "Nello Carrara," CNR, Florence, Italy.

⁵Dipartimento di Fisica, Università di Roma "La Sapienza," Rome, Italy.

⁶Istituto di Metodologie per l'Analisi Ambientale, CNR, Potenza, Italy.

⁷CETEMPS, Dipartimento di Fisica, Università di L'Aquila, L'Aquila, Italy.

⁸Department of Physics and Astronomy and Institute for Terrestrial and Planetary Atmospheres, State University of New York at Stony Brook, Stony Brook, New York, USA.

[4] Although in the last few years new humidity sensors mounted on radiosondes have proven to be a reliable tool for measuring atmospheric humidity in cold and dry conditions [Miloshevich *et al.*, 2006; Vömel *et al.*, 2007], radiosonde observations are limited in daily temporal coverage because of the economic and personnel efforts required for each launch. Moreover, the sonde ascent time limits the time resolution of PWV measurements to no less than 30 min, whereas water vapor content in the troposphere can vary significantly on a shorter time scale. Measurements of low amounts of PWV carried out regularly during the day and with a higher time resolution than balloon sondes can provide are necessary, for example, in monitoring upper tropospheric water vapor, its transport and rate of variation, or at sites devoted to atmospheric and astronomic observations within spectral regions (infrared, millimetric and submillimetric wavelengths) where water vapor is the dominant source of atmospheric opacity [e.g., Calisse *et al.*, 2004].

[5] In this study we present a technique for measuring precipitable water vapor using a Ground-Based Millimeter wave Spectrometer (GBMS) and compare its results with in situ and ground-based remote sensing correlative measurements. Although the technique is not new [see de Zafra *et al.*, 1983], the primary field campaign of the ECOWAR (Earth Cooling by Water vapor Radiation) project [Bhawar *et al.*, 2008] provided a unique opportunity for an intercomparison of accuracy against several other data sets. The ECOWAR campaign took place at Breuil-Cervinia (45.9°N, 7.6°E, elevation 1990 m) and Plateau Rosa (also known as Testa Grigia; 45.9°N, 7.7°E, elevation 3490 m, less than 7 km apart from Breuil-Cervinia), Italy, from 3 to 16 March 2007. It is part of an experimental program aimed at studying spectral properties of water vapor in its rotational band (17–50 μm), with particular attention to the water vapor continuum and line absorption parameters. Observations of spectrally resolved radiances between 100 and 1100 cm^{-1} were realized using two Fourier transform spectrometers: the REFIR-PAD (Radiation Explorer in the Far Infrared–Prototype for Applications and Development) [Palchetti *et al.*, 2006] installed at Plateau Rosa and the Fourier transform infrared (FTIR)/ABB Bomem [Esposito *et al.*, 2007] installed only a few km away at Breuil-Cervinia. Ancillary measurements of temperature and relative humidity were performed by the University of Basilicata Raman lidar system (BASIL) [Di Girolamo *et al.*, 2004] based at Breuil-Cervinia, and by Vaisala RS92k radiosondes launched from the same location. The GBMS provided water vapor column measurements and stratospheric ozone profiles from Plateau Rosa. In the next section we describe the GBMS observing technique used to measure atmospheric opacity at millimeter wavelengths, in section 3 the conversion from GBMS opacity measurements to PWV is discussed, while in section 4 a description of the various correlative water vapor measurements is provided. Sections 5 and 6 are dedicated to illustrate results obtained comparing the various data sets and to summarize our work.

2. GBMS Observing Technique

[6] The Ground-Based Millimeter wave Spectrometer (GBMS) measures rotational emission spectra of atmospheric chemical species such as O_3 , N_2O , CO and

HNO_3 , as well as the H_2O continuum, with a spectral window of 600 MHz tunable between approximately 230 and 280 GHz (or 7.7 and 9.3 cm^{-1}). It was designed and built at the Physics and Astronomy Department of the State University of New York at Stony Brook and comprises a front end receiver employing a cryogenically cooled SIS (Superconductor-Insulator-Superconductor) double sideband mixer with an intermediate frequency (IF) of 1.4 GHz. The back end is composed of an Acousto-Optical Spectrometer (AOS) with a spectral band pass of 600 MHz and a maximum resolution of 65 kHz [de Zafra, 1995]. The combination of the front and back ends results in the GBMS observation of two superimposed 600 MHz spectral windows whose center frequencies are separated by 2.8 GHz (two times the IF). At the AOS, the full 600 MHz spectrum is read in 40 ms and integrated over time at a computer. Each spectral file is saved after a total time integration of 5 to 15 min. In general, observed emission lines are too weak to display a good signal-to-noise ratio (S/N) within these short time integrations, and spectral files are usually added together off-line to reach a satisfactory S/N ratio. The GBMS observes the emission line of one chemical species at a time, usually for 1 to 5 h (depending on S/N). Its 600 MHz window must then be tuned to a different frequency interval (in the 230–280 GHz range) in order to observe the emission line of another chemical species.

[7] Given the physical parameters of a specific rotational transition, its spectral line shape depends strongly on the vertical concentration profile of the observed species (typically unknown) and on the atmospheric pressure profile (typically known). Therefore, by means of the observed line shape together with pressure and temperature vertical profiles, a mathematical deconvolution process allows finding the emitting molecule's concentration as a function of altitude. The overall spectral band pass and resolution of the GBMS are key elements to determine the 17–75 km altitude range where trace gases concentration can be measured [e.g., see Muscari *et al.*, 2007, and references therein]. For water vapor, we do not observe an H_2O emission line (e.g., at 183 or 325 GHz) but rather the emission from the H_2O continuum existing between emission lines. Therefore, only the integrated column contents can be obtained from GBMS observations of water vapor.

[8] During normal data taking operations the GBMS observes radiation from two different directions 75° to 80° apart, switched by a rotating reflective semicircular chopper wheel at ≈ 1 Hz frequency (see Figure 1). One observing direction is near the zenith (reference beam, or R) while the other points between 10° and 15° above the horizon (signal beam, or S). A dielectric sheet (made of Plexiglas) mounted in the R beam acts as a local partially transparent (and weakly emitting) “grey body” source of broadband radiation to compensate for the lower total power received from atmospheric emission near the zenith (with a shorter geometrical path length with respect to the S-beam), and allows a power balance to be achieved between the S and R beam directions. Different dielectric sheets are used, depending on atmospheric conditions, with their opacity ranging from ~ 0.2 to 0.8 Nepers at 275 GHz. This power balance is sensed by a phase-sensitive detector synchronized to the rotation of the beam-switching chopper wheel, and main-

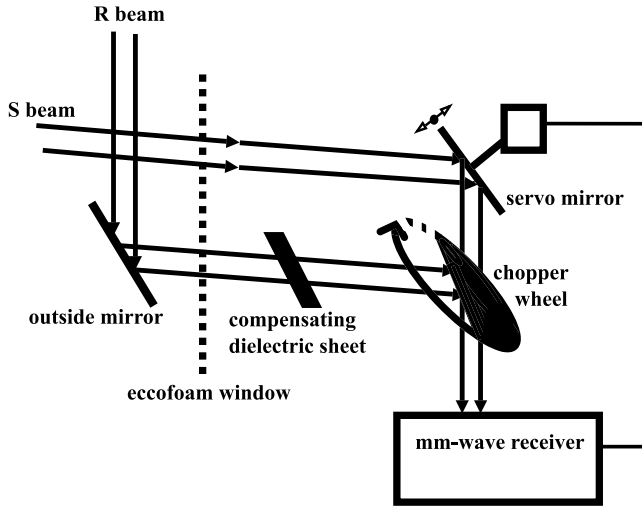


Figure 1. Schematic diagram of the GBMS front end. The inclination angle of the servo mirror is adjusted in order to keep the S and R powers balanced. The chopper wheel is a reflective half circle rotating with a $\simeq 1$ Hz frequency in order to let through to the receiver the S and R beams, alternatively. See text for details.

tained by a servo system which adjusts the elevation angle of the S beam if the (S-R) power level deviates from zero. As atmospheric opacity increases or decreases (causing thermal emission from the atmosphere to increase or decrease), the servo mechanism, seeking to maintain power balance in the two beams, will drive the S-beam angle upward or downward. The opacity of the dielectric sheet, dependent on its composition and thickness, will determine the equilibrium angles for a given range of atmospheric opacity. Atmospheric radiation from both beam directions enters through a window made of type PP-2 Eccof foam (see Figure 1) characterized by a very small opacity at millimeter wavelengths (~ 0.007 Nopers).

[9] As long as the emitting layer is optically thin, the signal intensity in S or R will be proportional to the geometrical path length (hereafter referred to as path length) through the layer. We define the air mass factor A_x as the dimensionless ratio of the path length along the x direction divided by the path length in the zenith direction z. For a spherical atmosphere one obtains

$$A_x = \frac{dx}{dz} = (r + z_H) \left/ \left[(r + z_H)^2 - (r + z_0)^2 \cos^2 \theta_x \right]^{1/2} \right., \quad (1)$$

where r is the Earth's radius, z_H the mean height of a thin layer above the Earth's surface, z_0 the altitude of the observer and θ_x is the angle of the observed path along the x direction measured from the horizontal. For $z_H < r$, $A_x \simeq 1/\sin \theta_x$, i.e., the relationship for a plane parallel atmosphere. In the present case, where the major contribution to atmospheric opacity arises from water vapor not bound in ice crystals, confined to a layer of mean height z at most few kilometers above the 3.5 km altitude of Plateau Rosa, the approximation $A_x \simeq 1/\sin \theta_x$ is within 2% of the full expression for $\theta_x = 10^\circ$ and less than 2% for larger values of θ_x .

[10] The following analysis determines the relationship between opacity and S-beam angle [e.g., *de Zafrá*, 1995]. The total power (expressed in temperature units) observed in the S direction at the frequency ν is:

$$T_s(\nu) = T_z^*(\nu) A_s \exp(-A_s \tau_z - \tau_w) + 2T_{CB} \exp(-A_s \tau_z - \tau_w) + 2T_w [1 - \exp(-\tau_w)] + 2T_{atm} [1 - \exp(-A_s \tau_z)] \exp(-\tau_w) + T_{rec}(\nu), \quad (2)$$

where A_s is the air mass factor in the S direction, $T_z^*(\nu)$ is the integrated signal intensity due to stratospheric and mesospheric molecular emission in the zenith direction (which we assume can be transformed to the molecular emission along any other line of sight by multiplying by A_x , i.e., we assume the atmospheric homogeneity), τ_z is the opacity of the atmosphere in the zenith direction (which, again, we assume can be transformed to the opacity along any other line of sight by multiplying by A_x). T_{CB} represents the emission due to the cosmic background, $T_{rec}(\nu)$ is the receiver noise, and T_w and τ_w are the physical temperature and opacity of the window material, respectively. T_{atm} is the mean physical temperature of the noise-radiating atmosphere, typically that of the first few km within the troposphere containing most of the water vapor. It gives rise to a broadband signal (no spectral features) with the properties of a uniform noise source over the 600 MHz spectral window. T_{atm} is obtained using local averaged temperature and water vapor lapse rates which determine a relationship between T_{atm} and the temperature monitored at the ground (there is no requirement of high accuracy on T_{atm} estimates). In equation (2), the frequency dependence is indicated only for those parameters which can vary significantly within the 600 MHz GBMS band pass. The remaining parameters (e.g., τ_z) are essentially constant over the band pass although they can vary over the 230–280 GHz range. Factors of 2 in equation (2) take into account the use of a double sideband receiver, with equal gain in each sideband. A factor of 2 is already hidden in the definition for $T_{rec}(\nu)$ for a double sideband receiver. Terms involving $\exp[-\tau_x]$ represent attenuation of signal by some entity along the path whose total opacity is τ_x , while terms involving $T_x(1 - \exp[-\tau_x])$ represent emission by the same entity, assumed to be at a mean physical temperature T_x . An expression similar to equation (2) gives the output power from the R direction:

$$T_R(\nu) = T_z^*(\nu) A_R \exp(-A_R \tau_z - \tau_p - \tau_w) + 2T_{CB} \exp(-A_R \tau_z - \tau_p - \tau_w) + 2T_{atm} [1 - \exp(-A_R \tau_z)] \exp(-\tau_p - \tau_w) + 2T_p [1 - \exp(-\tau_p)] + 2T_w [1 - \exp(-\tau_w)] \exp(-\tau_p) + T_{rec}(\nu), \quad (3)$$

where terms have been added to represent signal attenuation by the compensating sheet and its broadband emission for a given opacity τ_p and physical temperature T_p .

[11] During normal data taking operations the S and R output powers averaged over the two 600 MHz sideband spectral windows (whose center frequencies are 2.8 GHz apart) are balanced. Terms due to emission from the

Eccofoam window (those in T_w), the cosmic background (T_{CB}) and, when considering spectral averages over the 600 MHz band pass, terms due to molecular emission from stratospheric and mesospheric trace gases (those involving T_z^*) are negligible compared to other terms and we have:

$$\begin{aligned} T_{\text{atm}}[1 - \exp(-A_s \tau_z)] \exp(-\tau_w) \\ \simeq T_{\text{atm}}[1 - \exp(-A_R \tau_z)] \exp(-\tau_p - \tau_w) \\ + T_p[1 - \exp(-\tau_p)]. \end{aligned} \quad (4)$$

[12] In the above equation, all terms but τ_z can be derived from independent measurements so that the opacity in the zenith direction remains the only unknown quantity. In fact, all terms but A_S (directly derivable from a measure of θ_S) and τ_z are typically constant over a few hours and equation (4) shows that τ_z can be continuously derived from the record of the angle θ_S at which S and R powers are balanced during observation. Equation (4) can be solved for τ_z by means of an iterative procedure. The accuracy for the resulting τ_z values is estimated at 4.5% by adding in quadrature the uncertainties on θ_S (2.2%), T_{atm} (3.3%) and τ_p (2.2%). T_p is monitored by means of a temperature sensor placed next to the compensating sheet and averaged over 15-min periods. The resulting uncertainty has a negligible effect on τ_z .

[13] There is a second method to measure the opacity in the zenith direction, τ_z , and this involves measuring the sky brightness temperature in the S direction averaged over the 600 MHz band pass, T_{Ssky} . This is obtained by considering the total power of equation (2) (averaged over both sidebands) without the receiver noise temperature T_{rec} and the Eccofoam window terms. Again, neglecting very small contributions from stratospheric molecular line emission and from the cosmic background, T_{Ssky} is given by the expression:

$$T_{\text{Ssky}} = T_{\text{atm}}[1 - \exp(-\tau_z A_S)]. \quad (5)$$

Considering that the portion of the air mass factor affecting atmospheric opacity lies within a few km of the observer, where a plane parallel approximation for path length is quite accurate, we may take $A_S \sim 1/\sin\theta_S$. Then, solving for the zenith opacity τ_z leads to

$$\tau_z = -\sin\theta_S \cdot \ln\{1 - T_{\text{Ssky}}/T_{\text{atm}}\}, \quad (6)$$

where T_{Ssky} can be evaluated from locally measurable quantities by means of the GBMS calibrating procedure which is periodically carried out by the operator [*de Zafra*, 1995; *Parrish et al.*, 1988].

[14] This second procedure for the evaluation of τ_z is carried out by interrupting the normal data taking operations and performing a so-called ‘‘sky dip’’ [see, e.g., *Han and Westwater*, 2000]. The operation consists of manually moving the mirror which determines the S direction of observation within the range allowed by the window opening (~ 10 – 15° above the horizontal) at $\sim 0.5^\circ$ steps, mea-

suring the output power at each step by means of the GBMS, and estimating τ_z at each step using equation (6). If water vapor density is independent of viewing direction (atmospheric homogeneity) and T_{atm} has been estimated correctly, the derived values of τ_z will be in good agreement with one another and their average value will result in an estimate of zenith opacity. A further check on the horizontal homogeneity of the water vapor field is performed by measuring τ_z also at the zenith (after removing the compensating sheet normally placed in the R beam direction) and verifying its consistency with sky dip measurements. Using this technique, the uncertainty on each single measurement of τ_z (i.e., equation (6) applied to each single 0.5° mirror step) is estimated at 15%, with the largest relative error contribution of 14% coming from the uncertainty on the measurement of T_{Ssky} by means of the GBMS calibrating procedure. However, taking the mean of the ~ 11 τ_z measurements from the same sky dip results in a relative uncertainty on the mean τ_z of 5.1%. Although SIS mixers are sensitive to the polarization of the incident radiation, potential spurious changes of polarization (e.g., those caused by changing the orientation of the S beam mirror [e.g., *Renbarger et al.*, 1998]) are negligible compared to the unpolarized tropospheric signal observed by the GBMS between 230 and 280 GHz.

[15] Results from the two different methods described above are compared in the next section (see Figure 4), after discussing their conversion to PWV. Overall, the method based on balancing S and R output powers is preferred over the sky dip mainly because the former gives continuous measurements of opacity during normal observing of rotational emission lines. This means that τ_z measurements do not require the presence of an operator and each measurement can in principle be obtained with ~ 1 -min temporal resolution (allowing for the average of a large number of chopper rotations at 1 Hz frequency). The sky dip technique is instead carried out manually by the operator in about 15 min. Although the sky dip method takes somewhat into account potential spatial nonhomogeneity by averaging over a range of directions (albeit limited), at the same time it can be more affected by water vapor temporal variations with respect to the power balance method.

[16] The double sideband design of the GBMS is the limiting factor for the spectral resolution of τ_z measurements. Emission terms present in equations (4) and (6) are averages over two superimposed 600 MHz spectral windows (the upper and lower sidebands) whose center frequencies are separated by 2.8 GHz, giving rise to an overall 4 GHz resolution.

3. From GBMS Opacity Measurements to Precipitable Water Vapor

[17] In the 230–280 GHz spectral region the atmospheric emission arises almost entirely from water vapor continuum in cloud-free skies, with second-order contributions from molecular nitrogen and oxygen [e.g., see *Klein and Gasieweski*, 2000, Figure 1], and rotational spectra of trace gases contribute a negligible amount to the total brightness temperature observed by the GBMS, except for a few of the strongest O_3 emission lines. The conversion from the atmospheric opacity τ_z (measured at the various frequencies

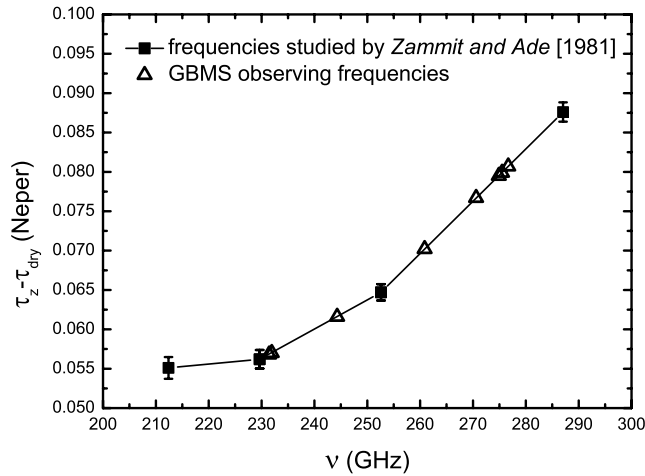


Figure 2. Opacity due to water vapor absorption only measured by *Zammit and Ade* [1981] at selected frequencies between 212 and 300 GHz (solid squares) and used in this work at the GBMS operating frequencies (open triangles). Plotted opacity values are for 1 mm of PWV.

where the GBMS is operated) to water vapor column content can hence be obtained by means of the linear relation:

$$\text{PWV} = [\tau_z(\lambda) - \tau_{\text{dry}}(\lambda)] \alpha(\lambda). \quad (7)$$

[18] Factors $\alpha(\lambda)$, which convert to PWV the opacity due to H_2O only, have been obtained from measurements carried out by *Zammit and Ade* [1981], while $\tau_{\text{dry}}(\lambda)$ values at Plateau Rosa are obtained using the radiative transfer (RT) model discussed by *Liljegren et al.* [2005]. Although we use the model scheme of *Liljegren et al.* [2005] only to estimate $\tau_{\text{dry}}(\lambda)$, we note that $\alpha(\lambda)$ and $\tau_{\text{dry}}(\lambda)$ values can differ significantly depending on the RT model considered. However, while differences on $\tau_{\text{dry}}(\lambda)$ have a limited effect on estimates of PWV, differences in modeled $\alpha(\lambda)$ factors can have a much larger impact. Hence our choice of relying on $\alpha(\lambda)$ values from the experimental data set of *Zammit and Ade* [1981] rather than adopting results from any of the RT models discussed in the literature (see below).

[19] *Zammit and Ade* [1981] derived experimental relationships to correlate τ_z with PWV at selected frequencies between 212 and 408 GHz, with a spectral resolution of 9.6 GHz. In order to derive $\alpha(\lambda)$ values at the GBMS frequencies of observation, a linear interpolation between the two closest frequencies investigated by *Zammit and Ade* [1981] was performed, as shown in Figure 2. We implemented these interpolations also using higher degree polynomials but obtained no substantial difference in the comparisons results shown in section 5. Furthermore, matching values of PWV are obtained from GBMS opacity measurements at different frequencies when they are carried out within a short time span (less than 15 min), suggesting that the conversion factors used are at least consistent with one another. This check can be performed when the GBMS

is returned in frequency in order to carry out daily measurements of different molecular species. Often, for example, the GBMS is first set to observe the CO line at 230.5 GHz and then moved in frequency to O_3 at 276.9 GHz, therefore measuring τ_z and PWV at frequencies $\simeq 46$ GHz apart within a short time span.

[20] The choice of using $\tau_{\text{dry}}(\lambda)$ values from *Liljegren et al.* [2005] originated from comparing factors $\alpha(\lambda)$ from *Zammit and Ade* [1981] with results from 5 different RT models [*Liebe and Layton*, 1987; *Liebe et al.*, 1993; *Rosenkranz*, 1998, 1999, 2003; *Liljegren et al.*, 2005]. We found that modeled $\alpha(\lambda)$'s from *Liljegren et al.* [2005] had the closest match to the *Zammit and Ade* [1981] experimental data (the former values being smaller by 6–9% at the GBMS observing frequencies) and chose their modeled $\tau_{\text{dry}}(\lambda)$ values for consistency. In Figure 3, $\tau_{\text{dry}}(\lambda)$ results from the 5 different RT models are plotted. Their 1σ standard deviation at each frequency (~ 0.003 mm, see Figure 3) is used as estimated uncertainty on the correspondent $\tau_{\text{dry}}(\lambda)$ value from *Liljegren et al.* [2005].

[21] As discussed by *Hewison et al.* [2006], *Liljegren et al.* [2005] proposed few modifications to previous millimeter wave propagation models (e.g., those discussed by *Liebe and Layton* [1987] and *Rosenkranz* [1998, 1999]) following recent results obtained from spectral atmospheric measurements. These modifications can be summarized in the use of parameters from the HITRAN database [*Rothman et al.*, 2003] and the MT_CKD continuum [*Clough et al.*, 2005].

[22] Uncertainties on GBMS PWV values are estimated by propagating the uncertainties on τ_z (see previous section), on $\tau_{\text{dry}}(\lambda)$, and the $\simeq 1.9\%$ error on $\alpha(\lambda)$'s [see *Zammit and Ade*, 1981]. This results in PWV uncertainties that vary from $\sim 5\%$ (for large PWV) to $\sim 10\%$ (for the smallest PWV observed), with very little dependence on the specific technique used to measure τ_z (i.e., sky dip or power balance).

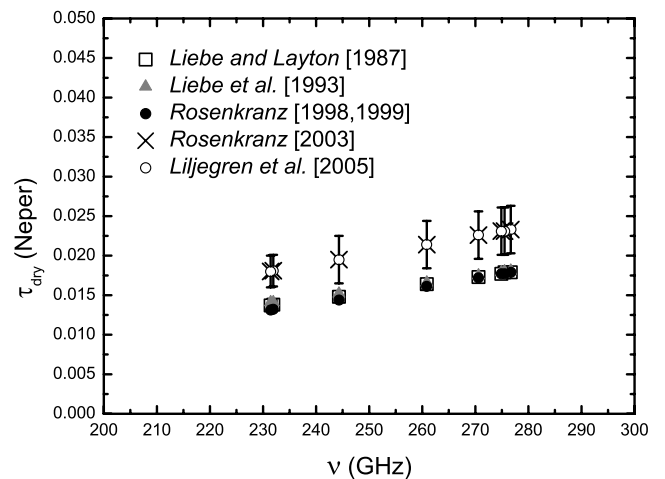


Figure 3. Opacity in the zenith direction due to a dry atmosphere as calculated by five different radiative transfer models (see text and legend) at the GBMS operating frequencies. The modeled opacity values assume a ground station at 3500 m altitude. Error bars indicate the 1σ standard deviation at each frequency calculated from the corresponding 5 τ_{dry} values.

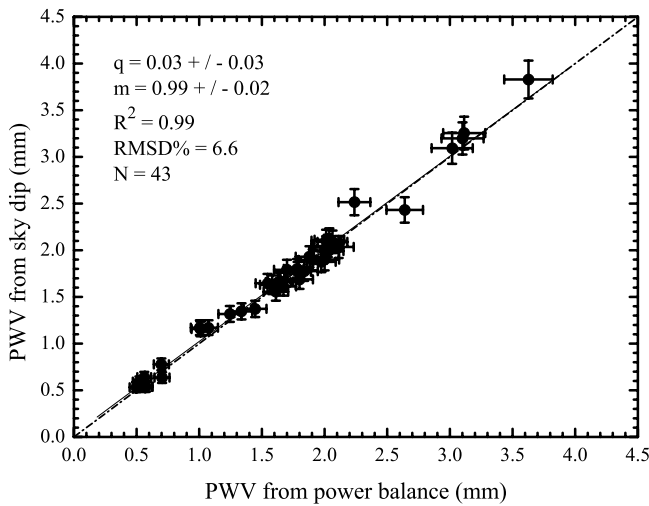


Figure 4. Scatterplot of PWV values obtained by balancing the S and R powers (x axis) versus PWV measured using a sky dip procedure (y axis, see text for details). The linear fit to the data points ($y = q + mx$) is represented with a solid line, and the 1:1 bisector is represented with a dash-dotted line. The percentage root mean square of the difference (RMSD%, see text) between the two sets of observations is also reported in the legend together with the total number of correlation points N, the parameters q and m of the linear fit, and the correlation coefficient R^2 .

[23] In Figure 4, PWV values obtained from GBMS opacity measurements carried out using the two different techniques at the same frequency within a short time span (less than 15 min) are compared. Figure 4 shows that a very

good agreement between the two sets of GBMS PWV values exists, with a percentage value of the root mean square of the difference (RMSD%) between the two data sets of 6.6%. Here we indicate with RMSD% the quantity

$$\text{RMSD}\% = \sqrt{\sum_i^N \frac{1}{N} \left[\frac{(x_i - y_i)}{x_i} 100 \right]^2}$$

, with x_i and y_i indicating the two sets of measurements being compared. The RMSD% represents a measure of the averaged discrepancy between two data sets, with the squared differences between pairs of data points insuring that positive and negative differences do not partly cancel out. Its comparison with data sets uncertainties indicates the level of agreement between the two sets of measurements.

[24] In Figure 5 the time series of precipitable water vapor values estimated by GBMS during the ECOWAR field campaign is shown. All values are obtained using the power balance method (see section 2). Measurements were carried out during the entire period of the ECOWAR campaign except in cases of poor weather conditions or occasional equipment malfunctioning. Although measurements from instruments participating to the ECOWAR campaign are used to characterize the environmental conditions occurring during GBMS operations, GBMS PWV values do not depend on data from the other PWV sets of measurements presented in this intercomparison study.

[25] Lidar and radiosonde measurements did provide the necessary information for evaluating potential influences of ice clouds on radiances measured at millimeter waves [e.g., *Evans and Stephens, 1995; Liu and Curry, 1998*]. Lidar measurements were used to detect the presence of clouds and, together with radiosonde relative humidity data, provided information on the cloud particles phase, which is

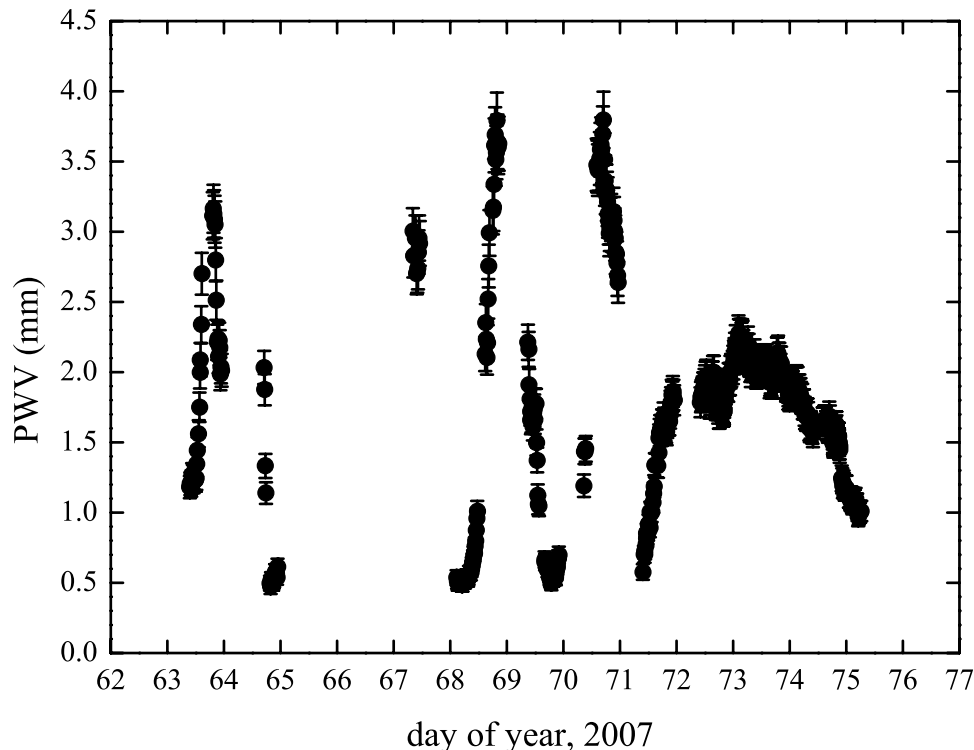


Figure 5. Time series of GBMS PWV during the ECOWAR field campaign at Plateau Rosa. Plotted values are those obtained from the power balance technique only.

Table 1. Vaisala RS92k Sensor Technical Data^a

	Range	Resolution	Total Uncertainty in Sounding
Temperature	−90°C to +60°C	0.1°C	0.5°C
Humidity	0% to 100%	1%	5%
Pressure	3–1080 hPa	0.1 hPa	0.6–1 hPa

^aThe accuracy is the 2-sigma confidence level (95.5%), including repeatability, long-term stability, measurement conditions effects, and response time [Jauhainen and Lehmuskero, 2005; Währn et al., 2004].

indicated to be always solid at the time of the GBMS observations discussed here. Lidar measurements of cirrus clouds optical depth at 532 nm (τ_{532}) provided a means for estimating an upper limit on ice water path (IWP) [Liou, 1992]. On the basis of lidar measurements of τ_{532} less than 1 (IWP at most ~ 0.04 mm) at the time of GBMS observations, we find that the occasional presence of cirrus clouds in the GBMS field of view can affect the observed T_{atm} by amounts that are well within its 3.3% uncertainty [e.g., see Cimini et al., 2007, Figure 8].

4. Correlative Water Vapor Measurements

4.1. RS92k Sonde

[26] During the 14-day-long ECOWAR field campaign, 34 Vaisala RS92k radiosonde units were launched from Cervinia and measured vertical profiles of atmospheric temperature and water vapor. Two to 4 sondes were launched each day from 4 to 15 March, except on 6 March when meteorological conditions prevented any data-taking from ground-based instruments. Data from 27 sondes were used in this study, with only 7 sondes launched during daytime (SZA < 85°). The sonde ascending time from the Cervinia field station (1990 m altitude) to ≈ 10 km altitude was approximately 20–25 min.

[27] The Vaisala RS92k radiosonde is equipped with temperature, pressure and humidity sensors (see technical data in Table 1 [Jauhainen and Lehmuskero, 2005]), while altitude information is obtained from the application of the hypsometric equation. Type k of the Vaisala radiosonde RS92 family is not equipped with a wind sensor. The advanced HUMICAP humidity sensor is composed of two thin-film capacitors that are alternatively heated in order to avoid ice formation on them at low temperatures and condensation of water vapor during sounding. The advanced HUMICAP sensor works on the principle of absorption of water molecules into the thin-film surface. Absorption of other molecules can contaminate the sensor and produce a bias in humidity measurements. In order to reduce this potential bias, a reconditioning procedure was performed on the radiosondes by heating the humidity sensor just before sounding therefore removing the contaminants from the sensor surface [Hirvensalo et al., 2002; Währn et al., 2004]. The reconditioning procedure was performed by using the Vaisala Ground Check Set GC25 that reads the original calibration coefficients automatically to assure that chemical contaminants have been removed.

[28] The RS92 radiosondes are commercially available since October 2003. Their operational characterizations took place in November 2003, during the Atmospheric

Infrared Sounder (AIRS) Water Vapor Experiment–Ground (AWEX-G) [Miloshevich et al., 2006], and in July 2005, during the observation campaign Ticosonde 2005 [Vömel et al., 2007]. During these campaigns, water vapor measurements by sondes RS92 were compared to simultaneous measurements carried out using the Cryogenic Frostpoint Hygrometer and, only during AIRS/AWEX-G, also using different radiosonde types. These studies pointed out that the humidity sensor mounted on RS92 sondes is the most accurate among those installed in four types of radiosonde currently produced by Vaisala (RS80-A, RS80-H, RS90, RS92). The RS92 model uses the same polymer humidity sensor employed in the older RS80-H but the size and thickness of the polymer layer is smaller, improving the sensor response time at low temperature [Miloshevich et al., 2004, 2006]. Moreover, the calibration process is more accurate than in previous models [Paukkunen et al., 2001]. The main problem for RS92 sondes lies in the lack of a radiation shield (present in RS80-H), which makes the RS92 sensor more susceptible to solar heating and produces a strong solar radiation dry bias [Vömel et al., 2007]. However, the magnitude of this radiation dry bias and its dependence on SZA is not yet well established [e.g., Miloshevich et al., 2004, 2006; Vömel et al., 2007; Rowe et al., 2008]. In their Figure 10, Rowe et al. [2008] plot several estimates of the radiation dry bias obtained in recent studies. From their Figure 10, we deduce that an 8% dry bias could be affecting the 7 daytime RS92k sondes used in this study and therefore applied this correction to the corresponding PWV values. Following the results depicted by Vömel et al. [2007] in their Figure 9, we assign an accuracy of 5% to PWV measurements obtained using RS92 sondes.

[29] In performing the comparison between GBMS and RS92k sonde PWV measurements (see section 5), radiosonde values were calculated by integrating water vapor concentrations from the pressure level of Plateau Rosa up to 10 km altitude. Integrating sonde measurements up to 15 km produces negligible differences. The corresponding GBMS PWV value is obtained from GBMS measurements carried out while radiosondes ascent from 3.5 km to 10 km altitude.

4.2. Raman Lidar BASIL

[30] Lidar measurements were performed by the University of Basilicata Raman lidar system (BASIL). The system was substantially upgraded prior the ECOWAR measurement campaign with the implementation of an additional receiver (developed at the University of Roma “La Sapienza”) dedicated to the detection of echoes from the lowest altitude levels. The major feature of BASIL is represented by its capability to perform high-resolution and accurate measurements of atmospheric temperature, both in daytime and nighttime, based on the application of the rotational Raman lidar technique in the UV [Di Girolamo et al., 2004]. Besides temperature, BASIL is capable of providing measurements of particle backscatter at 355, 532 and 1064 nm, particle extinction and depolarization at 355 and 532 nm, and water vapor mixing ratio vertical profiles both in daytime and nighttime. This wide range of measured parameters makes this system particularly suited for the study of meteorological processes and the characterization of aerosol and cloud microphysical properties.

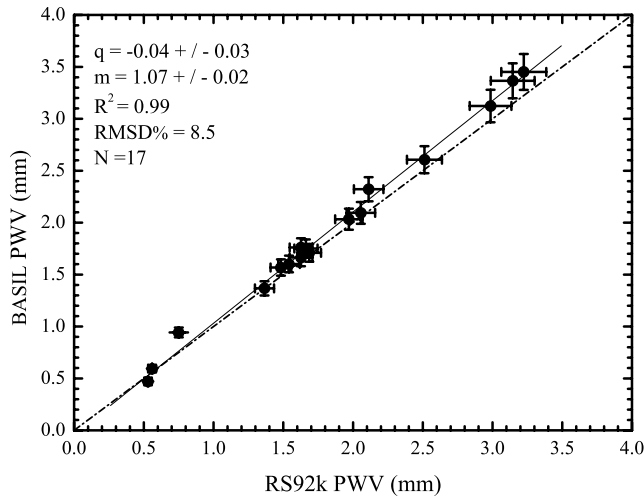


Figure 6. Scatterplot of BASIL versus Vaisala RS92k PWV measurements. Both lidar and sonde PWV amounts are obtained by integrating humidity measurements from the Plateau Rosa pressure level to 10 km altitude. The linear fit to the data points ($y = q + mx$) is represented with a solid line, and the 1:1 bisector is represented with a dash-dotted line. The RMSD% (see text) is also reported in the legend together with the total number of correlation points N , the parameters q and m of the linear fit, and the correlation coefficient R^2 .

[31] Vertical and temporal resolutions of raw data are 30 m and 1 min, respectively. However, in order to reduce signal statistical fluctuations, time integration together with vertical profile smoothing are applied to the data. For a time resolution of 5 min and a vertical resolution of 150 m, daytime measurements uncertainties at 2 km altitude are typically 5% for the particle backscattering coefficient (at all wavelengths), 20% for the particle extinction coefficient, 10% for water vapor mixing ratio values and 2 K for temperature values. Relative uncertainties for nighttime measurements at 2 km are half as much as daytime measurements for all parameters.

[32] BASIL calibration for water vapor measurements was achieved using simultaneous and colocated radiosonde observations. Once calibrated, BASIL water vapor measurements represented a key contribution to the field campaign by providing continuous vertical profiles of water vapor. The calibration constant was determined comparing BASIL and radiosondes water vapor mixing ratio values in the lowermost kilometer above Cervinia using all 34 launches performed during ECOWAR. The selection of the lowermost kilometer ensures that both instruments were sampling the same air mass during the calibration procedure. The consideration of all available radiosondes for the determination of the calibration constant used in this intercomparison effort prevents the dependence of a single lidar vertical profile from the simultaneous radiosonde profile.

[33] The use of a very compact optical design reduces significantly the differences between the overlap functions of the H_2O and N_2 Raman signals used to estimate water vapor mixing ratio. Nevertheless, differences in the lower 1500 m between the two overlap functions may, in principle,

be quantified through the application of the “ N_2 calibration procedure” [Whiteman *et al.*, 1992], consisting in the use of N_2 Raman filters in both the H_2O and N_2 channels. This calibration procedure was applied during ECOWAR at the beginning and end of each measurement session. However, small discrepancies have been revealed between overlap-corrected lidar and colocated radiosonde measurements, probably resulting from polarization effects originated in the dichroic beamsplitters used for the partitioning of the signals. Hence, an independent estimate of the overlap function ratio was obtained from the comparison of lidar and colocated radiosonde measurements. This procedure was applied to all radiosonde launches available during each measurement session and a mean overlap function ratio was determined for each measurement session. Variability of the overlap function during each measurement session was found to be very limited, with a very reduced impact on the PWV uncertainty (estimated to not exceed 3–5%).

[34] Water vapor lidar measurements used in this work are integrated over 10 min and have a vertical resolution of 150 m from the ground (≈ 2 km altitude) to 5 km and of 300 m above 5 km altitude. BASIL PWV values compared to GBMS values in the next section are obtained using only nighttime measurements. BASIL water vapor vertical profiles were integrated in the altitude region 3.5–10 km altitude. Although a 50% maximum uncertainty in mixing ratio values is reached at the uppermost altitude levels, this has little impact on total PWV estimates. The resulting BASIL PWV values have an estimated relative uncertainty of only 5%.

[35] In Figure 6, a comparison between values of PWV obtained from simultaneous radiosonde and lidar measurements is shown. Both sets of PWV values are computed integrating the water vapor content from 3.5 to 10 km altitude, as previously described, for consistency with comparisons discussed in section 5. Since BASIL calibration is based on RS92k humidity measurements between 2 and 3 km altitude, while all PWV values refer to the 3.5–10 km altitude range, concurrent lidar and sonde PWV measurements can, in practice, differ. Setting the upper limit for the PWV integration at an altitude of 10 km reduced the number of concurrent measurements that could be used for this comparison, since not all of the 34 radiosondes launched or the corresponding lidar profiles reached 10 km altitude. Figure 6 shows that a good agreement between the two sets of PWV values exists, with a RMSD% of 8.5%.

[36] Moreover, we quantified how many concurrent lidar and sondes measurements are consistent within their uncertainties. In other words, defining $\Omega_i = \Delta x_i + \Delta y_i - |x_i - y_i|$, being x_i, y_i a pair of concurrent measurements from the two data sets and $\Delta x_i, \Delta y_i$ the corresponding 1σ uncertainties, we find that in 87.5% of the cases (15 out of 17) Ω_i is positive; that is, the two measured PWV values are consistent within their uncertainties.

4.3. REFIR-PAD

[37] REFIR-PAD (Radiation Explorer in the Far Infrared–Prototype for Applications and Development) is a Fourier transform spectroradiometer measuring the spectrum of the downward longwave radiation (DLR) emitted from the atmosphere in the wide spectral range from 100 to

1400 cm^{-1} with a maximum resolution of 0.25 cm^{-1} . It is a prototype developed as a field demonstrator of a spaceborne instrument designed for the characterization of the Earth's radiation budget in the far infrared region [Palchetti *et al.*, 2005; Bianchini *et al.*, 2006]. REFIR-PAD was specifically designed with the requirements of reliability, light weight (55 kg) and low power consumption (about 50 W average) to fly on board stratospheric balloons [Palchetti *et al.*, 2006], but its extremely flexible design makes it suitable also for ground-based observations with only minor changes required [Bianchini *et al.*, 2007].

[38] The instrument uses an innovative optical design [Carli *et al.*, 1999] with two input ports and two output channels. One input port is used for looking at the unknown scene to be measured and the second one for looking at a reference blackbody source, which allows the access and the control of the instrument self-emission. At the output ports, signals are acquired with two room temperature DLATGS (deuterated L-alanine-doped triglycene sulfate) pyroelectric detectors.

[39] During the ECOWAR campaign, REFIR-PAD was operated in the 100–1100 cm^{-1} spectral range with 0.5 cm^{-1} spectral resolution and an acquisition time of 64 s for a single scan [Bhawar *et al.*, 2008]. Measurements contain the spectral signature of the pure rotational water vapor band and can be used for the characterization of the water vapor content in the atmosphere and in particular for the measurement of PWV.

[40] Measured DLR spectra are analyzed through a retrieval code based on the ARTS forward model [Buehler *et al.*, 2005] and a χ^2 minimization algorithm based on the MINUIT function minimization routines supplied by CERN [James, 1994]. The number of degrees of freedom (DOF) in the acquired data is determined through the analysis of the Jacobian of water vapor and temperature observations [Bianchini *et al.*, 2007]. To this purpose, first of all the Jacobian matrix is calculated as a function of wave number and altitude. Calculations are performed for zenith sounding, operating conditions at Plateau Rosa, and with a midlatitude winter standard atmosphere. The spectral range used for analysis is 305–650 cm^{-1} , the altitude range is from the ground to 18 km altitude.

[41] Singular values decomposition (SVD) is then applied to the Jacobian matrix. The relative magnitude of the resulting eigenvalues is used as a criterion to choose fitted parameters. The highest value is obtained for the first water vapor eigenvector, the second and third eigenvalues of water vapor are $\sim 3.5\%$ and $\sim 0.4\%$, respectively, of the first eigenvalue. For the atmospheric temperature, the first and second eigenvalues are 2.7% and 0.1%, respectively, of the first water vapor eigenvalue. As expected, the far-infrared spectral range shows a high sensitivity to water vapor atmospheric content. Given the $\sim 1\%$ average uncertainty on the measured radiance, we deduce a $\text{DOF} = 3$, with two DOF for water vapor and one for temperature.

[42] The chosen parameter set includes two points from the water vapor profile, about 1 km and 2 km above the measuring station of Plateau Rosa, and the temperature corresponding to the lowest water vapor fitted point. While the two values of the water vapor vertical profile are being

adjusted by the minimization algorithm, the rest of the profile is assumed to have the shape of the midlatitude winter standard water vapor profile and is rescaled accordingly.

[43] Practically, these two points represent two partial water vapor column contents that added together give the PWV. The midlatitude winter standard atmosphere temperature profile is instead rescaled according to the fitted temperature value and to the tropopause temperature of the standard profile. A very simple cloud model, based on the Rayleigh scattering approximation, is used to run retrievals in the presence of a thin cloud cover. The cloud geometry (layer altitude and thickness, cloud particles phase) is inferred from meteorological data, while the ice or liquid water content is fitted as an additional parameter. It is worth mentioning that REFIR-PAD measurements are always carried out when no visible clouds are present, so clouds affecting REFIR-PAD spectral measurements can only be subvisible cirrus clouds. Furthermore, water vapor and cirrus clouds have different effects on REFIR-PAD measurements: while clouds produce the effect of a reduced transparency in the windows between water vapor lines, leaving absorption lines unaffected, water vapor variations show up in absorption lines. These two different effects are not correlated and are adjusted independently (using different parameters) in the REFIR-PAD PWV retrieval procedure. Only two REFIR-PAD PWV data points used in this study are obtained in the presence of subvisible cirrus clouds, and they are relative to measurements carried out on 4 and 9 March.

[44] Since the first water vapor eigenvalue is more than one order of magnitude larger than the second water vapor and temperature eigenvalues, and the first water vapor eigenvector accounts for most of the total integrated water column, it follows that PWV is the physical parameter to which REFIR-PAD zenith-looking spectra show the largest sensitivity. This is taken into account in the estimation of the uncertainty on PWV values. Since most of the uncertainty on the two retrieved water vapor mixing ratio values comes from the correlation between them, which does not affect the total water vapor column, a second data analysis run is performed with only one fitted water vapor parameter. As expected from the SVD analysis described above, this procedure gives total column values that are overestimated or underestimated by up to a few percent (depending on atmospheric conditions), but their relative error does not have any contribution from the correlation between the two water vapor levels.

[45] Following the analysis described above, a 5% average relative uncertainty is assigned to measured PWV values. This 5% value encompasses more than 90% of the measurement errors obtained, with no visible dependence on PWV values.

[46] In this work, we use REFIR-PAD spectral measurements integrated over $\simeq 5$ min and retrieve a PWV value from each 5-min integration. In particular, REFIR-PAD PWV values reported in the following section are averages of 3 PWV retrievals obtained from 3 successive 5 min spectral integrations carried out concurrently with a sonde's ascent from 3.5 to 10 km altitude. The estimated uncertainty of 5% assigned to REFIR-PAD PWV values does not take into account the averaging procedure over 3 successive

PWV retrievals and is therefore to be considered a rather conservative accuracy assessment.

5. Comparisons Results

[47] In this section we compare precipitable water vapor values estimated using the GBMS with those obtained from the three additional sets of data described in the previous

section and obtained during the March 2007 ECOWAR field campaign. Comparisons are shown in three different scatterplots (Figures 7a–7c). GBMS estimates are those obtained using the power balance method (see section 2). Although this technique can in principle provide opacity measurements with a temporal resolution of ≈ 1 min, in practice GBMS raw measurements are integrated over 15 min during regular data taking. During the ECOWAR campaign we also carried out 5 min integrations at frequencies where no emission line of stratospheric and mesospheric chemical species could be detected and observations were devoted to opacity (and therefore PWV) measurements only.

[48] GBMS PWV measurements are in good agreement with the other three data sets displaying RMSD% values ranging from 9% to 9.6%. Furthermore, Ω_i values (see section 4.2) are positive in 78.5% of the cases for GBMS/lidar, 75% of the cases for GBMS/REFIR comparisons and in 86.9% of the cases for the GBMS/sonde comparison. The statistics reported in Figure 7 provide details for each comparison. In particular, the comparison between GBMS and BASIL data (Figure 7b) is based on a considerable number of correlation points and allows an interpretation of slope and intercept values of the linear fit to the scatterplot. A slope of $0.99 (\pm 0.02)$ indicates that the sensitivity of the two instruments to variations of PWV is within 1% ($\pm 2\%$) of one another. Alternatively, we can indicate slope and intercept values of the linear fit as measures of percentage and absolute systematic differences between GBMS and BASIL PWV measurements. This would lead to an estimation of percentage and absolute systematic differences of 1% ($\pm 2\%$) and $0.03 (\pm 0.02)$ mm, respectively.

[49] Although the same analysis can in principle be applied also to the comparisons illustrated in Figures 6, 7a, and 7c, a much smaller number of data points is available in these cases. For these correlation plots, we restrain from drawing any conclusion on the basis of the characteristics of the linear fits and consider RMSD% values the most accurate measure of the agreement between the data sets.

[50] The four comparisons illustrated in Figures 6 and 7 are not based on measurements all carried out at the same time. Each comparison relies, in principle, on separate pairs of measurements (i.e., each pair carried out at different times with respect to the other comparisons). In particular, the GBMS/lidar correlation is based on many points (31 out of 42) unique to the GBMS/lidar correlation and not available to the other three. This explains the apparent inconsistency among the slopes that characterize the lidar/sonde, GBMS/lidar, and GBMS/sonde correlations (see Figure 7).

[51] A systematic GBMS high bias appears to be present for measurements carried out on 13 March and marked in

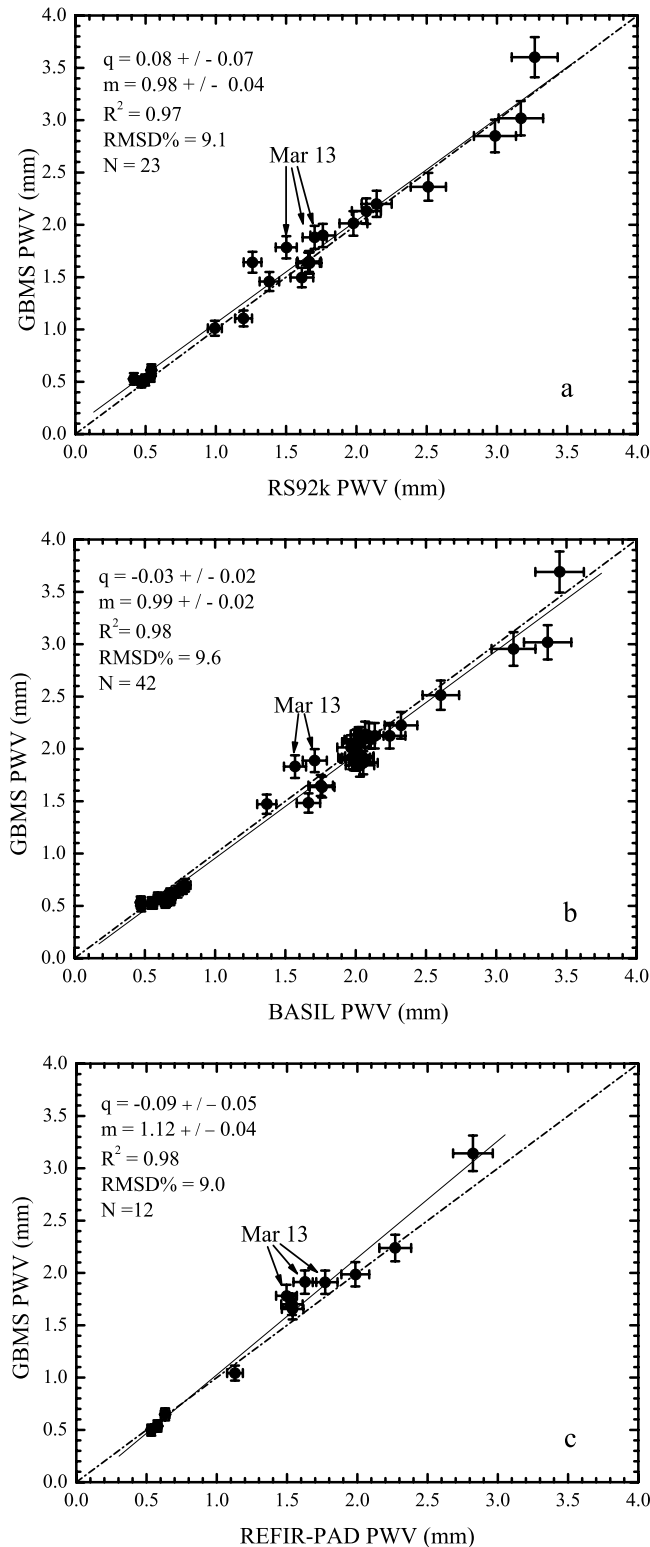


Figure 7. Scatterplot of (a) GBMS versus Vaisala RS92k, (b) GBMS versus BASIL, and (c) GBMS versus REFIR-PAD PWV amounts. Linear fits to the data points ($y = q + mx$) are represented in each panel with a solid line, and the 1:1 bisectors are represented with dash-dotted lines. The RMSD% (see text) for each comparison is also reported in the corresponding panel together with the associated total number of correlation points N, the parameters q and m of the corresponding linear fit, and the correlation coefficient R^2 .

Figure 7. During this day only, GBMS PWV are consistently larger than values from all other data sets by up to 16%. Although a large unaccounted inaccuracy in GBMS opacity observations for 13 March cannot be ruled out, this result, unique for 13 March, suggests that a peculiar meteorological condition possibly occurred on this day. Particle backscatter lidar measurements (not shown) indicate that a large amount of Saharan dust particles arrived over Cervinia on 12 March, reaching altitudes as high as 8 km. Concurrently, the GBMS PWV time series displayed in Figure 5 shows a rapid increase of the PWV (day 71, 12 March) from 0.6 mm at 0930 local time to 1.7 mm at 1900 local time, suggesting that the advection of lower tropospheric air from the Saharan region brought both desert aerosols and a large concentration of water vapor to the Western Alps. On 13 March, the Saharan aerosol layer slowly faded away and its top altitude was observed by BASIL at 4.5 km in the morning, lowering to ≈ 3 km in the late evening/night, while the GBMS PWV from Plateau Rosa stayed stable between 1.7 and 2 mm (see Figure 5). Since the GBMS opacity measurements from Plateau Rosa are based on observations at $10\text{--}15^\circ$ above the horizon looking almost directly north, while Cervinia is southwest of Plateau Rosa, during the particular transitional conditions of 13 March the GBMS might have sampled air masses with a different water vapor content relative to BASIL and the RS92k sondes, based at Cervinia, and even with respect to REFIR-PAD observing in the zenith direction from Plateau Rosa.

6. Summary

[52] Low amounts of PWV are difficult to measure accurately because of the necessary high instrumental sensitivity to water vapor, but are important for climate studies, in particular for correctly modeling longwave fluxes in polar regions, for increasing our basic knowledge about concentration and transport of water vapor in the upper troposphere and in polar regions, and for providing ancillary information to atmospheric and astronomy observations performed at infrared, millimetric and submillimetric wavelengths. In this study we describe a technique for measuring very low column contents of water vapor (below 4 mm of PWV) using observations of atmospheric opacity at frequencies between 230 and 280 GHz. Although the technique was developed by *de Zafra et al.* [1983], here we present the first accurate intercomparison of these measurements with in situ and ground-based correlative measurements. Furthermore, we use the state of the art radiative transfer model in the millimeter wavelength range by *Liljegren et al.* [2005] in order to take into account the opacity due solely to the dry atmosphere (not negligible under very low PWV conditions) with a resulting improvement with respect to the qualitative PWV estimates displayed by *de Zafra et al.* [1983] and *Parrish et al.* [1987].

[53] We discuss the two methods used to measure atmospheric opacity using the GBMS, the beam balancing and the sky dip procedures, and the scatterplot displayed in Figure 4 shows that the two methods produce the same results with similar accuracies. In order to obtain PWV amounts, we have first removed the component due to the dry atmosphere from the GBMS atmospheric opacity measurements and then applied a scale factor obtained from

measurements reported by *Zammit and Ade* [1981] to convert to PWV the opacity due to H_2O only.

[54] The intercomparison between the GBMS data set and simultaneous PWV observations obtained with Vaisala RS92k radiosondes, a Raman lidar, and an IR Fourier transform spectrometer is presented in section 5. These sets of concurrent measurements were carried out during the primary field campaign of the ECOWAR project which took place on the Western Italian Alps from 3 to 16 March 2007.

[55] GBMS PWV measurements are in good agreement with the other three data sets displaying percentage values for the root mean square of the difference between observations ranging from 9% to 9.6% (see Figure 7). Given the considerable number of data points available for the comparison between GBMS and lidar measurements, for this case we can provide an interpretation of slope and intercept values of the linear fit to the scatterplot (Figure 7b) which suggests very small, if any, systematic differences between the two data sets. The slope indicates a percentage systematic difference of 1% ($\pm 2\%$), while the intercept suggests an absolute systematic difference of 0.03 (± 0.02) mm.

[56] Only on 13 March were GBMS PWV values consistently larger than those from all other data sets by up to 16%. Although a large unaccounted inaccuracy in GBMS opacity observations carried out on 13 March cannot be ruled out, we discuss the possibility that a peculiar meteorological condition has taken place on this day.

[57] **Acknowledgments.** This research was carried out with a grant from MIUR PRIN 2005, project 2005025202/Area 02, and funding from NASA grant NAG 513029. We are indebted to the Istituto di Fisica dello Spazio Interplanetario (INAF/IFSI), the Centro Nazionale di Meteorologia e Climatologia Aeronautica (CNMA), and the town of Valtourneche (Breuil-Cervinia) for logistic support at the two field sites of Plateau Rosa and Cervinia. We thank Daniele Fuà and Giorgio di Sarra for helpful discussions. We also thank Dave Turner and two anonymous reviewers for valuable comments on the original manuscript.

References

- Bhawar, R., et al. (2008), Spectrally resolved observations of atmospheric emitted radiance in the H_2O rotation band, *Geophys. Res. Lett.*, *35*, L04812, doi:10.1029/2007GL032207.
- Bianchini, G., L. Palchetti, and B. Carli (2006), A wide-band nadir-sounding spectroradiometer for the characterization of the Earth's outgoing long-wave radiation, *Proc. SPIE Int. Soc. Opt. Eng.*, *6361*, 63610A.
- Bianchini, G., L. Palchetti, and A. Baglioni (2007), Far infrared spectrally resolved broadband emission of the atmosphere from Monte Morello and Monte Gomito near Florence, *Proc. SPIE Int. Soc. Opt. Eng.*, *6745*, 6745–6761.
- Buehler, S. A., P. Eriksson, T. Kuhn, A. von Engel, and C. Verdes (2005), ARTS, the atmospheric radiative transfer simulator, *J. Quant. Spectrosc. Radiat. Transfer*, *91*, 65–93, doi:10.1016/j.jqsrt.2004.05.051.
- Calisse, P. G., M. C. B. Ashley, M. G. Burton, M. A. Phillips, J. W. V. Storey, S. J. E. Radford, and J. B. Peterson (2004), Submillimeter site testing at Dome C, Antarctica, *Publ. Astron. Soc. Aust.*, *21*, 1–18, doi:10.1071/AS03018.
- Carli, B., A. Barbis, J. E. Harries, and L. Palchetti (1999), Design of an efficient broadband far-infrared Fourier-transform spectrometer, *Appl. Opt.*, *38*, 3945–3950, doi:10.1364/AO.38.003945.
- Cimini, D., E. R. Westwater, A. J. Gasiewski, M. Klein, V. Y. Leuski, and J. C. Liljegren (2007), Ground-based millimeter- and submillimeter-wave observations of low vapor and liquid water contents, *IEEE Trans. Geosci. Remote Sens.*, *45*, 2169–2180, doi:10.1109/TGRS.2007.897450.
- Clough, S. A., M. J. Iacono, and J.-L. Moncet (1992), Line-by-line calculations of atmospheric fluxes and cooling rates: Application to water vapor, *J. Geophys. Res.*, *97*(D14), 15,761–15,785.
- Clough, S. A., M. W. Shephard, E. J. Mlawer, J. S. Delamere, M. J. Iacono, K. Cady-Pereira, S. Boukabara, and P. D. Brown (2005), Atmospheric radiative transfer modeling: A summary of the AER codes, *J. Quant. Spectrosc. Radiat. Transfer*, *91*, 233–244, doi:10.1016/j.jqsrt.2004.05.058.

- de Zafra, R. L. (1995), The ground-based measurements of stratospheric trace gases using quantitative millimeter wave emission spectroscopy, in *Diagnostic Tools in Atmospheric Physics, Proc. of the Int. Sch. of Phys. "Enrico Fermi,"* vol. 124, 23–54, Soc. It. di Fis., Bologna, Italy.
- de Zafra, R. L., A. Parrish, P. M. Solomon, and J. W. Barrett (1983), A quasi continuous record of atmospheric opacity at $\lambda = 1.1$ mm over 34 days at Mauna Kea observatory, *Int. J. Infrared Millimeter Waves*, 4, 757–765, doi:10.1007/BF01009694.
- Di Girolamo, P., R. Marchese, D. N. Whiteman, and B. B. Demoz (2004), Rotational Raman lidar measurements of atmospheric temperature in the UV, *Geophys. Res. Lett.*, 31, L01106, doi:10.1029/2003GL018342.
- Esposito, F., G. Grieco, G. Masiello, G. Pavese, R. Restieri, C. Serio, and V. Cuomo (2007), Intercomparison among line-parameters spectroscopic databases using downwelling spectral radiance, *Q. J. R. Meteorol. Soc.*, 133, 191–202.
- Evans, K. F., and G. L. Stephens (1995), Microwave radiative transfer through clouds composed of realistically shaped ice crystals. Part II. Remote sensing of ice clouds, *J. Atmos. Sci.*, 52, 2058–2072, doi:10.1175/1520-0469(1995)052<2058:MRTCC>2.0.CO;2.
- Han, Y., and E. R. Westwater (2000), Analysis and improvement of tipping calibration for ground-based microwave radiometers, *IEEE Trans. Geosci. Remote Sens.*, 38, 1260–1277, doi:10.1109/36.843018.
- Held, I. M., and B. Soden (2000), Water vapor feedback and global warming, *Annu. Rev. Energy Environ.*, 25, 441–475, doi:10.1146/annurev.energy.25.1.441.
- Hewison, T. J., D. Cimini, L. Martin, C. Gaffard, and J. Nash (2006), Validating clear air absorption model using ground-based microwave radiometers and vice-versa, *Meteorol. Z.*, 15(1), 27–36, doi:10.1127/0941-2948/2006/0097.
- Hirvensalo, J., J. Wahrn, and H. Jauhainen (2002), New Vaisala RS92 GPS radiosonde offers high level of performance and GPS wind data availability, paper presented at 12th Symposium on Meteorological Observations and Instrumentation, Am. Meteorol. Soc., Long Beach, Calif.
- James, F. (1994), Minuit, function minimization and error analysis, reference manual, *CERN Program Libr. Long Writeup, D506*, Comput. and Networks Div., Eur. Organ. for Nucl. Res., Geneva, Switzerland.
- Jauhainen, H., and M. Lehmuskero (2005), Performance of the Vaisala radiosonde RS92-SGP and Vaisala DigiCORA sounding system MW31 in the WMO Mauritius radiosonde intercomparison, technical note, Vaisala Oyi, Helsinki. (Available at <http://www.vaisala.com/weather/products/soundingequipment/radiosondes/rs92/mauritiustest>)
- Klein, M., and A. J. Gasiewski (2000), Nadir sensitivity of passive millimeter and submillimeter wave channels to clean air temperature and water vapor variations, *J. Geophys. Res.*, 105(D13), 17,481–17,511, doi:10.1029/2000JD900089.
- Liebe, H. J., and D. H. Layton (1987), Millimeter-wave properties of the atmosphere: Laboratory studies and propagation modeling, *NPLA-Rep.*, 87–224, Natl. Telecommun. and Inf. Admin., Boulder, Colo.
- Liebe, H. J., G. A. Hufford, and M. G. Cotton (1993), Propagation modeling of moist air and suspended water/ice particles at frequencies below 1000 GHz, paper 542 presented at AGARD 52nd Specialists' Meeting of the Electromagnetic Wave Propagation Panel, Advisory Group for Aerospace Res. and Dev., Palma de Mallorca, Spain, 1–10 March.
- Liljegen, J. C., S.-A. Boukabara, K. Cady-Pereira, and S. A. Clough (2005), The effect of the half-width of the 22-GHz water vapor line on retrievals of temperature and water vapor profiles with a 12-channel microwave radiometer, *IEEE Trans. Geosci. Remote Sens.*, 43, 1102–1108, doi:10.1109/TGRS.2004.839593.
- Liou, K. N. (1992), *Radiation and Cloud Processes in the Atmosphere*, 487 pp., Oxford Univ. Press, New York.
- Liu, G., and J. A. Curry (1998), Remote sensing of ice water characteristics in tropical clouds using aircraft microwave measurements, *J. Appl. Meteorol.*, 37, 337–355, doi:10.1175/1520-0450(1998)037<0337:RSOIVC>2.0.CO;2.
- Marsden, D., and F. P. J. Valero (2004), Observation of water vapour greenhouse absorption over the Gulf of Mexico using aircraft and satellite data, *J. Atmos. Sci.*, 61, 745–753, doi:10.1175/1520-0469(2004)061<0745:OOWVGA>2.0.CO;2.
- Miloshevich, L. M., A. Paukkunen, H. Vömel, and S. J. Oltmans (2004), Development and validation of a time lag correction for Vaisala radiosonde humidity measurements, *J. Atmos. Oceanic Technol.*, 21, 1305–1327, doi:10.1175/1520-0426(2004)021<1305:DAVOAT>2.0.CO;2.
- Miloshevich, L. M., H. Vömel, D. N. Whiteman, B. M. Lesht, F. J. Schmidlin, and F. Russo (2006), Absolute accuracy of water vapour measurements from six operational radiosonde types launched during AWEX-G and implications for AIRS validation, *J. Geophys. Res.*, 111, D09S10, doi:10.1029/2005JD006083.
- Muscari, G., A. G. di Sarra, R. L. de Zafra, F. Lucci, F. Baordo, F. Angelini, and G. Fiocco (2007), Middle atmospheric O₃, CO, N₂O, HNO₃, and temperature profiles during the warm Arctic winter 2001–2002, *J. Geophys. Res.*, 112, D14304, doi:10.1029/2006JD007849.
- Palchetti, L., C. Belotti, G. Bianchini, F. Castagnoli, B. Carli, U. Cortesi, M. Pellegrini, C. Camy-Peyret, P. Jeseck, and Y. Té (2006), First spectral measurement of the Earth's upwelling emission using an uncooled wide-band Fourier transform spectrometer, *Atmos. Chem. Phys.*, 6, 5025–5030.
- Palchetti, L., G. Bianchini, F. Castagnoli, B. Carli, C. Serio, F. Esposito, V. Cuomo, R. Rizzi, and T. Maestri (2005), Breadboard of a Fourier-transform spectrometer for the Radiation Explorer in the Far Infrared atmospheric mission, *Appl. Opt.*, 44, 2870–2878, doi:10.1364/AO.44.002870.
- Parrish, A., R. L. de Zafra, J. W. Barrett, P. Solomon, and B. Connor (1987), Additional atmospheric opacity measurements at $\lambda = 1.1$ mm from Mauna Kea observatory, Hawaii, *Int. J. Infrared Millimeter Waves*, 8, 431–440, doi:10.1007/BF01013256.
- Parrish, A., R. L. de Zafra, P. M. Solomon, and J. W. Barrett (1988), A ground-based technique for millimeter wave spectroscopic observations of stratospheric trace constituents, *Radio Sci.*, 23, 106–118, doi:10.1029/RS023i002p0106.
- Paukkunen, A., V. Antikainen, and H. Jauhainen (2001), Accuracy and performance of the new Vaisala RS90 radiosonde in operational use, paper presented at 11th Symposium on Meteorological Observations and Instrumentation, Am. Meteorol. Soc., Albuquerque, N. M., 14–18 Jan.
- Raval, A., and V. Ramanathan (1989), Observational determination of the greenhouse effect, *Nature*, 342, 758–761, doi:10.1038/342758a0.
- Renbarger, T., J. L. Dotson, and G. Novak (1998), Measurements of sub-millimeter polarization induced by oblique reflection from aluminum alloy, *Appl. Opt.*, 37, 6643–6647, doi:10.1364/AO.37.006643.
- Rosenkranz, P. W. (1998), Water vapor microwave continuum absorption: A comparison of measurements and models, *Radio Sci.*, 33, 919–928, doi:10.1029/98RS01182.
- Rosenkranz, P. W. (1999), Correction to “Water vapor microwave continuum absorption: a comparison of measurements and models”, *Radio Sci.*, 34, 1025, doi:10.1029/1999RS900020.
- Rosenkranz, P. W. (2003), Rapid radiative transfer model for AMSU/HSB channels, *IEEE Trans. Geosci. Remote Sens.*, 41, 362–368, doi:10.1109/TGRS.2002.808323.
- Rothman, L. S., et al. (2003), The HITRAN molecular spectroscopic database: Edition of 2000 including updates through 2001, *J. Quant. Spectrosc. Radiat. Transfer*, 82, 5–44, doi:10.1016/S0022-4073(03)00146-8.
- Rowe, P. M., L. M. Miloshevich, D. D. Turner, and V. P. Walden (2008), Dry bias in Vaisala RS90 radiosonde humidity profiles over Antarctica, *J. Atmos. Oceanic Technol.*, doi:10.1175/2008JTECHA1009.1, in press.
- Solomon, S., D. Qin, M. Manning, Z. Chen, M. Marquis, K. B. Averyt, M. Tignor, and H. L. Miller (Eds.) (2007), *Climate Change 2007: The Physical Science Basis—Contribution of Working Group I to the Fourth Assessment Report of the Intergovernmental Panel on Climate Change*, 996 pp., Cambridge Univ. Press, Cambridge, U.K.
- Vömel, H., H. Selkirk, L. Miloshevich, J. Valverde-Canossa, J. Valdès, E. Kyrö, R. Kivi, W. Stolz, G. Peng, and J. A. Diaz (2007), Radiation dry bias of the Vaisala RS92 humidity sensor, *J. Atmos. Oceanic Technol.*, 24, 953–963, doi:10.1175/JTECH2019.1.
- Währn, J., I. Rekikoski, H. Jauhainen, and J. Hirvensalo (2004), New Vaisala radiosonde RS92: Testing and results from the field, paper presented at Eighth Symposium on Integrated Observing and Assimilation Systems for Atmosphere, Oceans, and Land Surface, Am. Meteorol. Soc., Seattle, Wash.
- Whiteman, D. N., S. H. Melfi, and R. A. Ferrare (1992), Raman lidar system for the measurement of water vapor and aerosols in the Earth's atmosphere, *Appl. Opt.*, 31, 3068–3082.
- Zammit, C. C., and P. A. R. Ade (1981), Zenith atmospheric attenuation measurements at millimetre and sub-millimetre wavelengths, *Nature*, 293, 550–552, doi:10.1038/293550a0.
- C. Bianchi, I. Fiorucci, and G. Muscari, Istituto Nazionale di Geofisica e Vulcanologia, I-00143 Rome, Italy. (fiorucci@ingv.it)
- G. Bianchini and L. Palchetti, Istituto di Fisica Applicata “Nello Carrara,” CNR, I-50127 Florence, Italy.
- M. Cacciani and T. Di Iorio, Dipartimento di Fisica, Università di Roma “La Sapienza,” I-00185 Rome, Italy.
- D. Cimini, CETEMPS, Dipartimento di Fisica, Università di L'Aquila, I-67010 L'Aquila, Italy.
- R. L. de Zafra, Department of Physics and Astronomy, State University of New York at Stony Brook, Stony Brook, NY 11794, USA.
- P. Di Girolamo, F. Esposito, G. Grieco, and D. Summa, Dipartimento di Ingegneria e Fisica dell'Ambiente, Università della Basilicata, I-85100 Potenza, Italy.
- G. Pavese, Istituto di Metodologie per l'Analisi Ambientale, CNR, I-85050 Potenza, Italy.